Optimum Aeroelastic Design of Helicopter Rotors for Longitudinal Handling Qualities Improvement

Roberto Celi*
University of Maryland, College Park, Maryland 20742

This paper describes an optimization study in which the torsional stiffness of a hingeless rotor blade and its cross-sectional offsets are designed to stabilize the phugoid oscillation of the aircraft by increasing the stabilizing effect of the rotor. The real part of the phugoid eigenvalues is minimized at a specified advance ratio, subject to aeroelastic stability constraints in forward flight, blade root peak-to-peak load constraints for flap bending and torsion, and a longitudinal cyclic response requirement. The aeroelastic analysis and the flight mechanics analysis are connected indirectly to the numerical optimization algorithm through the use of a sequence of approximate optimization problems. A new algorithm to generate a high quality set of starting vectors is presented. The results of the study show that the combined analysis/optimization program can generate designs that have stable phugoid modes and satisfy all the aeroelastic and flight mechanic constraints.

Nomenclature

a = lift curve slope of main rotor airfoil
a_t = lift curve slope of the tailplane
C_H = H-force coefficient
C_T = thrust coefficient
C_W = weight coefficient
c = blade chord
$\boldsymbol{D}$ = vector of design variables
$\nabla F(\boldsymbol{D})$ = gradient of objective function or behavior constraints
$f(\boldsymbol{D})$ = objective function
GJ = torsional stiffness of the blade
$\boldsymbol{g}(\boldsymbol{D})$ = vector of behavior constraints
$[H(\boldsymbol{D}_0)]$ = Hessian of objective function or behavior constraints
I_y = pitching moment of inertia of the helicopter
M = pitching moment acting on the helicopter
M_{xR} = peak-to-peak value of torsion moment at the root of the blade (rotating system)
M_{yR} = peak-to-peak value of flap bending moment at the root of the blade (rotating system)
N = number of design variables
N_b = number of blades
n = load factor
q = pitch angular velocity of the helicopter divided by Ω
R = rotor radius
T_F = time elapsed between step longitudinal cyclic pitch input and inflexion point of load factor time history
u = horizontal velocity perturbation of the helicopter
W = weight of the helicopter
w = vertical velocity perturbation of the helicopter
X,Z = horizontal and vertical forces acting on the helicopter
x_A = offset between the elastic axis and the aerodynamic center, positive for aerodynamic center ahead of the elastic axis.
x_I = offset between the elastic axis and the center of mass, positive for center of mass ahead of the elastic axis
ζ_j = real part of longitudinal stability eigenvalue
θ = pitch attitude of the helicopter
λ_j = longitudinal flight stability eigenvalue
μ = advance ratio
σ = rotor solidity, $= Nc/\pi R$
ω_j = imaginary part of longitudinal stability eigenvalue
Ω = main rotor speed
$()_P$ = quantity for phugoid mode
$()_u,()_w,()_q$ = stability derivative associated with perturbations in horizontal velocity, vertical velocity, and pitch rate, respectively
$()_{\theta_0},()_{\theta_{1s}}$ = control derivative associated with collective pitch and longitudinal cyclic pitch, respectively

Nondimensionalization Factors

Forces $= \rho\sigma A(\Omega R)^2$
Moments $= \rho\sigma AR(\Omega R)^2$

Introduction and Problem Statement

In recent years, there has been a growing interest in applications of numerical optimization to a variety of helicopter engineering problems. In particular, a relatively large number of studies concerning the optimization of helicopter rotors has been published recently. Most of these studies have dealt with the dynamic and aeroelastic optimization of the rotor for vibration and loads reduction. References 1–3 are representative of the state of the art in this area. Other areas that have been considered include aerodynamic optimization[4] and rotor performance optimization.[5]

Most rotor aeroelastic and aerodynamic analyses are not design oriented, that is, they are not capable of providing the sensitivity of rotor behavior with respect to given sets of design variables, in the form of analytic derivatives, as integral parts of the solution process. Reference 3 is an important first step in remedying this situation. The need remains, however, for techniques that allow the integration of non-design oriented rotor analyses in numerical optimization procedures, without incurring prohibitive computational

Presented as Paper 89-1270 at the AIAA/ASME/ASCE/AHS/ASC 30th Structures, Structural Dynamics and Materials Conference, Mobile, AL, April 3–5, 1989; received Jan. 20, 1990; revision received April 13, 1990; accepted for publication April 20, 1990.

*Assistant Professor, Center for Rotocraft Education and Research, Department of Aerospace Engineering. Member AIAA.

requirements. The techniques used successfully in the past are based on approximation concepts,[6] such as first- and second-order pseudo-Taylor series[7] expansions of objective function and behavior constraints,[2] or first-order Taylor series expansions.[8]

The main objective of this paper is to explore the possibility of integrating rotor aeroelasticity and helicopter flight dynamics in an interdisciplinary optimization process. The assumptions are made that both the aeroelastic and the flight dynamic analyses are not design oriented and that the cost of generating design sensitivity information is proportional to the number of design variables. The optimization procedure used in this paper allows considerable flexibility in the choice of design variables, objective function, and behavior constraints. However, this study will focus on a specific objective function, namely, the damping of the long period (phugoid) mode of the longitudinal flight dynamics of the helicopter. Therefore, numerical optimization will be used to select blade design parameters of a hingeless rotor so that rotor dynamic effects stabilize the phugoid mode, while at the same time the rotor is maintained free from aeroelastic instabilities. Additional constraints prevent the blade loads from increasing excessively during the optimization and enforce a typical cyclic pitch response requirement for the aircraft.

An additional objective of this paper is to describe an algorithm to generate a high-quality set of design vectors to start the optimization. In fact, the optimization algorithm used in this study requires a starting set of $N+1$ linearly independent but otherwise arbitrary design vectors and a corresponding set of objective function and behavior constraint values.[7] This starting set may already be available, for example, as the result of some previous parametric study. If no such information is available, the algorithm presented in this paper exploits the first $N+1$ analyses to try to generate a sequence of $N+1$ feasible and improving designs.

Solution Technique

Analysis

The analysis portion of this study is divided into two parts, namely, the analysis of the aeroelastic behavior of the rotor and the analysis of the longitudinal flight mechanics of the complete helicopter.

The aeroelastic analysis is described in detail in Refs. 9 and 10; only a brief outline is given below.

The rotor blade is modeled as an elastic beam undergoing flap, lag, and torsional deformations. The assumption of moderate deflections leads to kinematic nonlinearities in the equations of motion. The rotor hub can move with constant linear and angular velocities. The influence of hub kinematics on the aerodynamic and inertia loads is taken into account exactly. The partial differential equations of motion of the blade are transformed into a set of ordinary differential equations of motion using a finite element discretization, based on Galerkin method of weighted residuals. These equations are solved using a quasilinearization algorithm. An implicit formulation of the aerodynamic and inertial loads is used in the equations. This means that aerodynamic and inertial loads are built numerically during the iterative solution process using the approximate solution generated at the previous iteration. Thus, no symbolic algebraic manipulations are required to combine the various portions of the mathematical model. All the quantities of the inertia and aerodynamic mathematical model are automatically retained, regardless of how small they might be, thus eliminating the need for ordering schemes. The hub motions need not be small. A modal coordinate transformation based on the coupled, rotating normal modes of the blade is used to reduce the number of degrees of freedom of the problem. Six modes were used to derive all the results of this paper.

The aeroelastic calculations are coupled with the determination of the trim state of the complete helicopter.[11] For the purpose of the trim calculations, the nonlinear partial differential equations of motion of the blade are first transformed into a system of nonlinear ordinary differential equations using a finite element Galerkin method to eliminate the spatial variable. This system is then transformed into a system of nonlinear algebraic equations using a harmonic balance type procedure based on a global Galerkin method. The algebraic equations describing the force and moment equilibrium for the complete aircraft are appended to those describing the blade response, and the combined set is solved simultaneously.[11]

The classical quasisteady assumption of flight mechanics is assumed to hold. Thus, the stability and control derivatives are computed by perturbing the trim conditions one variable at a time.

The second part of the analysis portion of this study, namely, the longitudinal flight mechanics analysis of the helicopter, is based on the assumption that the lateral and the longitudinal motions are decoupled and on the small perturbation assumption.

Thus, the equations of motion are[12]

$$\begin{bmatrix} m & 0 & -X_q & 0 \\ 0 & m & 0 & 0 \\ 0 & 0 & 1 & 0 \\ 0 & -M_{\dot{w}} & 0 & 1 \end{bmatrix} \begin{Bmatrix} \dot{u} \\ \dot{v} \\ \dot{\theta} \\ \dot{q} \end{Bmatrix} = \begin{bmatrix} X_u & X_w & -W\sin\theta & 0 \\ Z_u & Z_w & -W\cos\theta & mV+Z_q \\ 0 & 0 & 0 & 1 \\ M_u & M_w & 0 & M_q \end{bmatrix} \begin{Bmatrix} u \\ w \\ \theta \\ q \end{Bmatrix} + \begin{bmatrix} X_{\theta_{1s}} & X_{\theta_0} \\ Z_{\theta_{1s}} & X_{\theta_0} \\ 0 & 0 \\ M_{\theta_{1s}} & M_{\theta_0} \end{bmatrix} \begin{Bmatrix} \theta_{1s} \\ \theta_0 \end{Bmatrix} \tag{1}$$

and can be written more compactly as

$$[E]\{\dot{y}\} = [\bar{F}]\{y\} + [\bar{G}]\{u\} \tag{2a}$$

$$\{\dot{y}\} = [F]\{y\} + [G]\{u\} \tag{2b}$$

with $[F] = [E]^{-1}[\bar{F}]$ and $[G] = [E]^{-1}[\bar{G}]$.

The longitudinal stability is determined from the eigenvalues of the matrix $[F]$. Usually $[F]$ has a complex conjugate pair of eigenvalues $\lambda_P = \zeta_P \pm i\omega_P$ corresponding to a low-frequency, unstable pitching oscillation (phugoid mode). The other pair of eigenvalues corresponds to a well-damped, short period mode. These eigenvalues may appear as a complex conjugate pair or as a real, negative pair.

Optimization

The optimization problem is cast in nonlinear mathematical programming form. Thus, the objective is to minimize a function $f(\boldsymbol{D})$ of a vector $\boldsymbol{D}$ of design variables, subject to a certain number of constraints $\boldsymbol{g}(\boldsymbol{D}) \leq 0$. Approximation concepts[6] are used. More specifically, the objective function and the behavior constraints are expanded in Taylor series in terms of the design variables:

$$F(\boldsymbol{D}) \approx F(\boldsymbol{D}_0) + \nabla F(\boldsymbol{D}_0)^T \delta\boldsymbol{D} + \tfrac{1}{2}\delta\boldsymbol{D}^T[H(\boldsymbol{D}_0)]\delta\boldsymbol{D} \tag{3}$$

where $F(\boldsymbol{D})$ is taken to be any objective or constraint function, $\boldsymbol{D}_0$ is the current design, and $\nabla F(\boldsymbol{D}_0)$ and $[H(\boldsymbol{D}_0)]$ are the gradient and the Hessian matrix at the current design, respectively. The Hessian matrix is the matrix of the second partial derivatives of the objective function with respect to the design

variables. The perturbation vector $\delta \boldsymbol{D}$ is defined as

$$\delta \boldsymbol{D} = \boldsymbol{D} - \boldsymbol{D}_0 \tag{4}$$

As in Ref. 2, pseudo-Taylor series expansions are actually used, following a technique introduced by Vanderplaats.[7] Thus, the Taylor series expansions defined by Eq. (3) are substituted by more general quadratic interpolation polynomials defined over a wider region of the design space, and the perturbation vector $\delta \boldsymbol{D}$ is not necessarily small. Only linear polynomials are required to start the optimization. Quadratic expressions can be progressively built as the optimization proceeds by using the various designs generated during the optimization process.

The design variables used in this optimization study are the torsional stiffness GJ, the offset x_A between the aerodynamic center (AC) and the elastic axis (EA) of the blade, and the offset x_I between the center of mass (CG) and the elastic axis of the blade. This particular choice is due to the fact that a lagged pitch rate feedback law, which can help stabilize the longitudinal dynamics of a helicopter, can be implemented through a proper dynamic design of the rotor.[13] This is accomplished by introducing chordwise offsets of the AC and of the CG of the blade. The stabilizing effect increases with decreasing blade torsional stiffness and increasing distance between the CG and the AC, with the CG placed in front of the AC.[13]

Side constraints are placed on the design variables to prevent them from reaching unphysical values, such as negative values for the stiffnesses or chordwise offsets larger than the blade chord. Side constraints may also be placed in the course of the optimization to implement move limits, which prevent the design variables from reaching regions of the design space in which the approximations to objective function and behavior constraints are judged not to be sufficiently accurate.

The objective function to be minimized is the real part ζ_P of the complex conjugate pair of eigenvalues corresponding to the phugoid mode at the advance ratio $\mu = 0.3$. This choice is due to the fact that forward flight has a destabilizing effect on the phugoid mode of a hingeless rotor helicopter, even in the presence of a horizontal tail.[12]

Three different types of behavior constraints, enforced at $\mu = 0.3$, are placed on the design:

Aeroelastic stability constraints. Reference 9 has shown that cross-sectional offsets of the centers of mass and aerodynamic centers may induce aeroelastic instabilities in forward flight, for both soft and stiff in-plane blades. Therefore, it is prudent to substitute the hover aeroelastic stability constraints of Ref. 2 with the forward flight constraints of the present study. If ζ_K is the real part of the characteristic exponent for the kth of the m generalized coordinates used to describe the blade,[2] then the aeroelastic stability constraints are expressed mathematically in the form:

$$g(\boldsymbol{D}) = \zeta_K \le 0, \qquad k = 1,2,\ldots,m \tag{5}$$

Blade root load constraints. Acting on the cross-sectional offsets of the blade to stabilize the longitudinal dynamics may increase the blade root loads, that is, the blade loads in the rotating system. Thus, the root load constraints express the requirement that the maximum peak-to-peak flap bending moment M_{yR} and the maximum peak-to-peak torsion moment M_{xR} at the blade root do not increase by more than preassigned fractions ΔM_y and ΔM_x, compared with their respective baseline values M_{yRB} and M_{xRB}. The root load constraints are expressed in the form:

$$g(\boldsymbol{D}) = [M_{yR}/(1 + \Delta M_y)M_{yRB}] - 1 \le 0 \tag{6}$$

$$g(\boldsymbol{D}) = [M_{xR}/(1 + \Delta M_x)M_{xRB}] - 1 \le 0 \tag{7}$$

Cyclic pitch response constraint. In order to insure acceptable maneuver stability characteristics, the military handling qualities specifications MIL-H-8501A requirements include that the time history of the load factor n following a step cyclic pitch input shall become concave downward within 2.0 s following the start of the maneuver.[14] The cyclic pitch response constraint considered in this study is representative of the MIL-H-8501A requirements and is expressed in the form:

$$g(\boldsymbol{D}) = T_F \le 2.0 \text{ s} \tag{8}$$

Equation (8) requires that $\ddot{n} = 0$ at a time $T_F \le 2.0$ s.

The second derivative $\ddot{n}$ of the load factor is obtained from the solution of Eq. (1) using the short period approximation[12]

$$\ddot{n}(t) = k_1 Z_w (a_1 e^{\lambda_1 \tau} + a_2 e^{\lambda_2 \tau}) \tag{9}$$

in which

$$a_1 = \frac{\lambda_1(\lambda_1 + \Gamma)}{\lambda_1 - \lambda_2}, \qquad a_2 = \frac{\lambda_2(\lambda_2 + \Gamma)}{\lambda_2 - \lambda_1} \tag{10}$$

and

$$k_1 = -\frac{Z_{\theta_{1s}}}{C_W/\sigma}, \qquad \tau = \frac{t}{\hat{t}}, \qquad \hat{t} = \frac{W}{g\rho\sigma\Omega^2 R^3} \tag{11}$$

$$\Gamma = -\frac{M_q}{i_y}, \qquad i_y = \frac{I_y}{WR^2/g} \tag{12}$$

In Eq. (9), λ_1 and λ_2 are the eigenvalues corresponding to the short period mode.

Optimum Design Process Organization

The organization of the optimum design process is shown schematically in Fig. 1. The analysis process begins with the calculation of the trim state of the aircraft and with an aeroelastic stability and response analysis for the rotor. The real parts of the characteristic exponents of the various modes, which indicate the aeroelastic stability levels and the peak-to-peak values of the bending and torsion loads at the

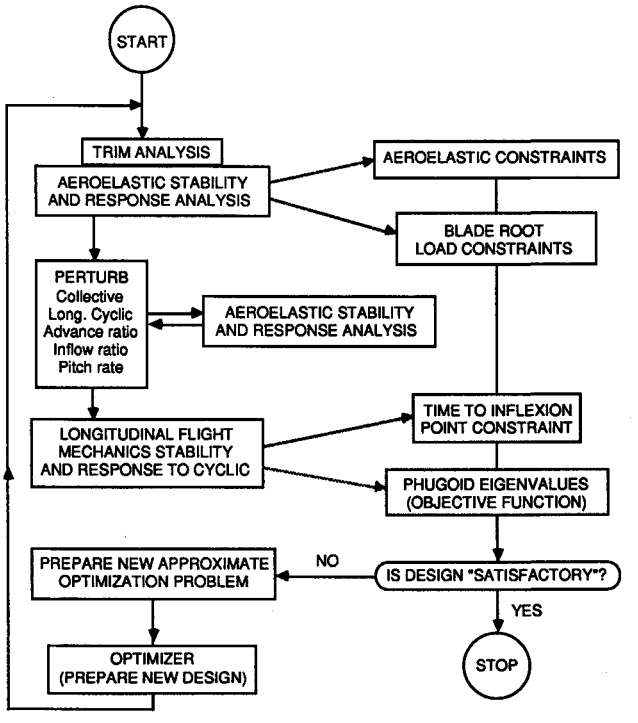

Fig. 1 Optimum design process organization.

blade root, are calculated in this phase. These two groups of parameters provide the information required to generate the aeroelastic stability constraints and the blade root load constraints, respectively.

The next step consists of the calculation of the rotor contributions to the stability and control derivatives of the aircraft. As mentioned previously, this is accomplished by perturbing each of the relevant variables, one at a time, and using finite difference approximations to compute the derivatives. The rotor contributions to the stability and control derivatives are then added to the airframe contributions, and both a longitudinal dynamic stability analysis and a calculation of the response to a step longitudinal cyclic pitch input are carried out. This provides the time required for the load factor curve to have an inflexion point and, thus, the value of the cyclic pitch response constraint. The real part of the complex conjugate pair of phugoid eigenvalues then yields the objective function.

At this point, the design is examined. If it is judged adequate, the design procedure is terminated. If it is not, either because one or more of the constraints are violated or because it appears possible to obtain further improvements, the design procedure continues. The design just analyzed is then added to all the previous designs and new approximations to the objective function and behavior constraints are obtained. In the next phase, the numerical optimization algorithm, in this case CONMIN,[15,16] solves this approximate constrained optimization problem and generates a new design. The new design is then analyzed and the cycle described in this section is repeated.

Determination of Starting Set of Design Vectors

If the number of design variables is large and the entire starting set of $N+1$ design vectors needs to be determined, one should try to choose the design vectors so as to achieve progress in the optimization, even before the starting set is complete. The idea behind the algorithm described in this section is that a set of k design vectors ($k \le N$) provides an approximate gradient and, thus, a search direction that can be used to determine an improved $k+1$ design.

Thus, the $k+1$ design $\boldsymbol{D}_{k+1}$, $k \le N$ is given by

$$\boldsymbol{D}_{k+1} = \boldsymbol{D}'_{k+1} + \boldsymbol{\delta}_{k+1} \tag{13}$$

in which $\boldsymbol{\delta}_k$ is a perturbation vector with all its elements equal to zero, except for the kth, which is equal to a given percentage of the kth design variable (in this study a perturbation of 10% was used). The vector $\boldsymbol{D}'_{k+1}$ is given by

$$\boldsymbol{D}'_{k+1} = \boldsymbol{D}_1 + [S]\boldsymbol{\alpha}^* \tag{14}$$

in which $[S]$ is a matrix with N rows and $k-1$ columns, the jth column of which is $\boldsymbol{S}_j = \boldsymbol{D}_j - \boldsymbol{D}_{j-1}$. The vector $\boldsymbol{\alpha}^*$ is a solution of the following constrained optimization problem:

$$\text{minimize } f(\boldsymbol{\alpha}) \tag{15}$$

subject to

$$g(\boldsymbol{\alpha}) \le 0 \tag{16}$$

Objective function and behavior constraints are identical to that of the main optimization problem and are expanded in first-order Taylor series in the components α_j, $j = 1,\ldots,k-1$ of the design variable vector $\boldsymbol{\alpha}$. It can be shown from Eq. (14) that the design vector $\boldsymbol{D}_j$ corresponds to $\alpha_1 = \alpha_2 = \cdots = \alpha_j = 1$, with the remaining $\alpha = 0$. Side constraints can be placed on the α. In the present study, the generic α_j cannot vary by more than 20% of its optimum value in the solution of the previous step.

It should be noted that it is not possible to use the set of $N+1$ vectors $\boldsymbol{D}'_k$ as a starting set because these vectors are not linearly independent. The perturbation vector $\boldsymbol{\delta}_k$ in Eq. (13) is intended to make the set of $N+1$ vectors $\boldsymbol{D}$ linearly independent. The vector $\boldsymbol{\delta}_{N+1}$ cannot be constructed in the same way as the other vectors $\boldsymbol{\delta}_k$. In this study, $\boldsymbol{\delta}_{N+1}$ is defined as

$$\boldsymbol{\delta}_{N+1,j} = 0.1[(S_{j,N})/|S_{j,N}|] \tag{17}$$

where $\boldsymbol{\delta}_{N+1,j}$ is the jth element of the vector $\boldsymbol{\delta}_{N+1}$. It is prudent to verify at each step the linear independence of the design vectors computed up to that step. This can be accomplished, for example, by constructing an N by $k+1$ matrix $[D]$, the columns of which are the design vectors, performing a singular value decomposition, and verifying that there are $k+1$ nonzero singular values of $[D]$.

It is convenient to use an additional function evaluation to start the algorithm. Then, given two arbitrary design vectors $\boldsymbol{D}_0$ and $\boldsymbol{D}_1$, the optimization problem just described is solved to find an improved design vector $\boldsymbol{D}_2$. The vector $\boldsymbol{D}_0$ is discarded and the process continues as indicated by Eqs. (13) and (14).

Results

This section contains the results obtained following the optimization procedure outlined in the previous sections. The results of three cases are presented in this section, namely, 1) optimization of a soft in-plane, uniform blade configuration; 2) optimization of a stiff in-plane, uniform blade configuration, and 3) generation of a starting set of design vectors for a nonuniform soft in-plane blade configuration. All blades have the same spanwise uniform mass distribution. The blade has no pretwist, root offset, droop, or precone. The rotor solidity σ is equal to 0.07. The fundamental, rotating coupled flap frequency is 1.12/rev when the cross-sectional offsets are set equal to zero.

The aircraft is assumed to be in straight, level, horizontal flight at $1g$ at an advance ratio $\mu = 0.3$ and a thrust coefficient $C_T = 0.005$. The center of mass of the aircraft is assumed to be at a distance $0.02R$ in front of the mast axis and $0.25R$ under the hub. The helicopter is equipped with a tailplane of area equal to $0.05\sigma a$ and lift curve slope $a_t = 4.5$.

Case 1: Soft In-Plane Blade Configuration

The first example refers to a soft in-plane blade configuration, with fundamental, rotating, coupled lag frequency of 0.73/rev when the cross-sectional offsets are set equal to zero. The three design variables used in this case are the torsional stiffness GJ, and the chordwise offsets x_A and x_I. Figures 2–7 show the iteration histories of objective function, design variables, and selected behavior constraints of the optimization problem.

The iteration history of the objective function is presented in Fig. 2. Designs 0–3 represent the initial set of $N+1$ design

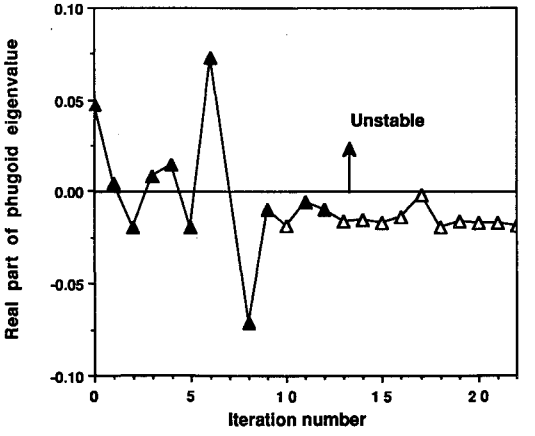

Fig. 2 Case 1—Iteration history of the objective function, soft in-plane blade configuration (solid symbols denote infeasible designs).

vectors required to start the optimization algorithm. Design 0 is the baseline, whereas designs 1, 2, and 3 are arbitrarily selected designs used to complete the set of $N+1$ vectors required to start the optimization. All four designs are infeasible because they violate the cyclic pitch response constraints. Two iterations of optimization failed to produce a design that exhibited such an inflexion point. Therefore, the next three designs (6, 7, and 8) were obtained by solving an unconstrained optimization problem in which the objective function to be minimized was the value of the second derivative $\ddot{n}$ of the load factor at time $t = 2$ s. The main optimization procedure was then restarted and generated all the remaining

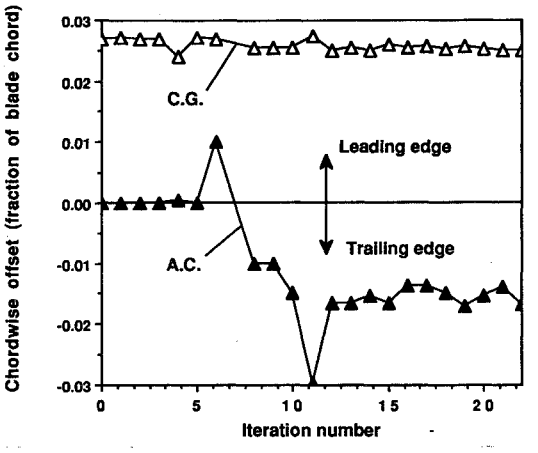

Fig. 3 Case 1—Iteration history of the blade chordwise offsets, soft in-plane blade configuration.

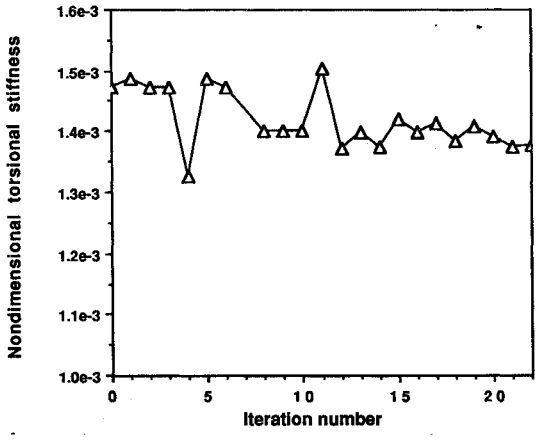

Fig. 4 Case 1—Iteration history of the blade torsional stiffness, soft in-plane blade configuration.

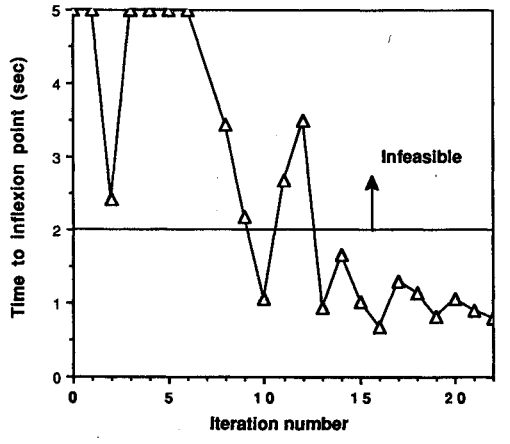

Fig. 5 Case 1—Iteration history of the time to inflexion point, soft in-plane blade configuration.

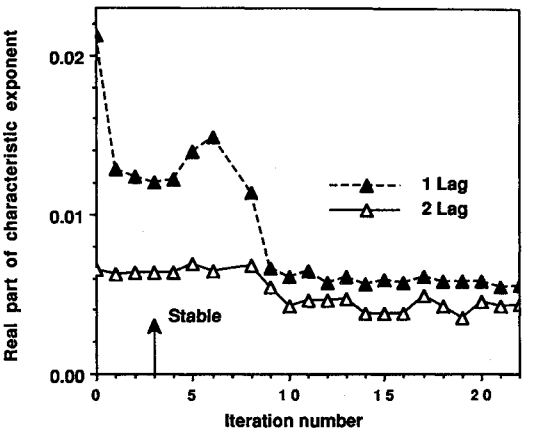

Fig. 6 Case 1—Iteration history of the damping of the first two lag modes, soft in-plane blade configuration.

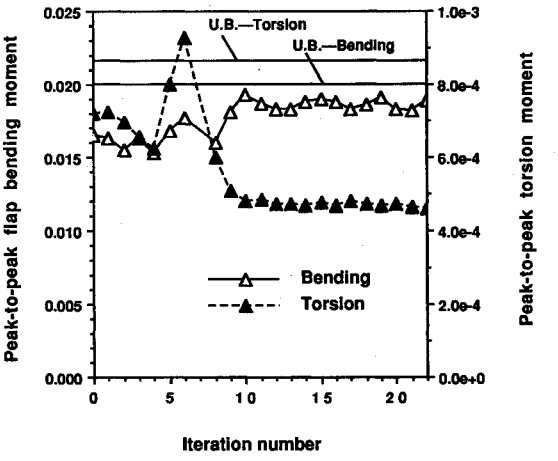

Fig. 7 Case 1—Iteration history of the peak-to-peak blade root loads, soft in-plane blade configuration.

design vectors. Starting from design 13, all the designs were feasible. Figure 2 shows that, after design 13, the optimization process leads to a sequence of slowly (but not monotonically) improving designs. The optimization was arbitrarily stopped at design 22. Throughout the optimization, move limits of $\pm 20\%$ were placed on the design variables.

Figure 3 shows that the optimizer leaves the CG of the blade at a distance of about 2.5% of the chord in front of the elastic axis. The elastic axis, instead, is moved ahead of the AC as the optimization progresses. From a zero or near zero value for the first six designs, the offset x_A increases to a final value of about -2% of the chord. The optimizer also decreases the torsional stiffness of the blade by about 10%, as shown in Fig. 4.

The iteration history of the cyclic pitch response constraint is presented in Fig. 5. It should be noted that an arbitrary value of $T_F = 5$ s was assigned for all the cases in which the time history of the load factor did not have an inflexion point at all. The aeroelastic stability of the first lag mode decreases considerably during the optimization process, as shown in Fig. 6. The stability of the second lag mode also decreases slightly. Both modes, however, remain stable. The stability level of the remaining four modes is much higher and is not affected by the optimization in a major way. Therefore, no data for these modes are presented here. The iteration history of peak-to-peak blade root loads is shown in Fig. 7. Stabilizing the phugoid through rotor aeroelastic tailoring leads to an increase of almost 20% of the peak-to-peak root bending loads. However, this increase remains below the prescribed upper bound, and the bending load constraint never becomes

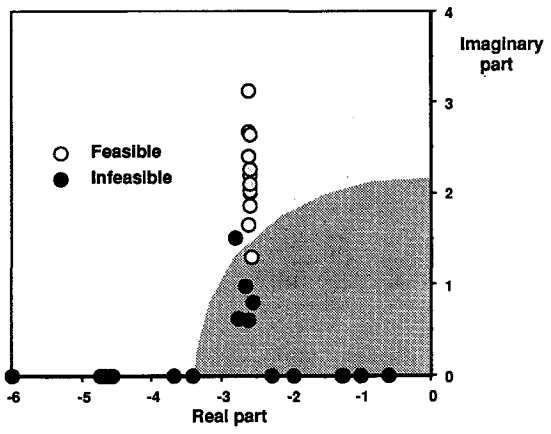

Fig. 8 Case 1—Short period poles of all the design generated during the optimization, soft in-plane blade configuration.

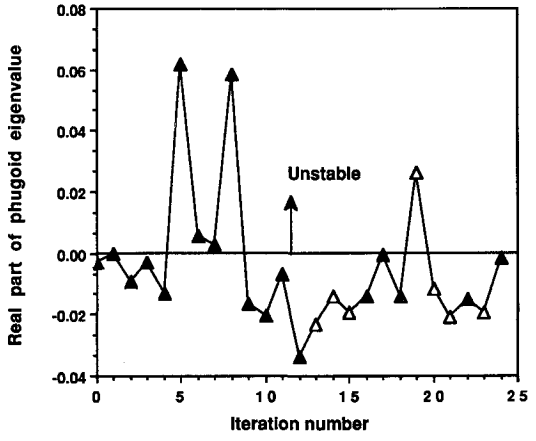

Fig. 9 Case 2—Iteration history of the objective function, stiff in-plane blade configuration (solid symbols denote infeasible designs).

active. Figure 7 also indicates that the peak-to-peak root torsion moments decrease as the optimization progresses.

It is interesting to note that the effects of the optimization resemble those of a pole placement procedure, as far as the flight dynamics poles are concerned. The minimization of the objective function is equivalent to pushing the phugoid poles as far to the left as possible in the s plane. Additionally, Fig. 8 shows that satisfying the cyclic pitch response constraint is equivalent to moving the short period poles outside an infeasible region of the s plane, which is drawn qualitatively as a shaded area in the figure. The precise boundaries of the infeasible region depend on selected aerodynamic stability derivatives[12] and, therefore, vary with the design.

Case 2: Stiff In-Plane Blade Configuration

The second example refers to a stiff in-plane blade configuration with fundamental, rotating, coupled lag frequency of 1.43/rev when the cross-sectional offsets are set equal to zero. As in case 1, the three design variables used in the optimization are the torsional stiffness GJ, and the chordwise offsets x_A and x_I. Figures 9–14 show the iteration histories of objective function, design variables, and selected behavior constraints of the optimization problem.

The iteration history of the objective function is presented in Fig. 9. As in case 1, designs 0–3 represent the initial set of $N+1$ design vectors required to start the optimization algorithm. Once again, design 0 is the baseline, and designs 1, 2, and 3 are arbitrarily selected to complete the initial set of $N+1$ design vectors. Both the initial four designs and the next nine generated by the optimizer are infeasible because the constraint on the aeroelastic stability of the second lag mode is violated. Designs 0–9 and 11 also violate the cyclic pitch response constraint. Design 13 is feasible and so are most of the subsequent designs up to design 24 when the optimization is arbitrarily stopped. Although the optimization process generates a number of good designs that improve considerably on the baseline design and are feasible, no clear convergence can be identified for the objective function, and some infeasible designs continue to be produced. Tight move limits of $\pm 10\%$ were placed on the design variables up to design 11. The limits were subsequently increased to $\pm 50\%$ for GJ and $\pm 5\%$ of the blade chord for the chordwise offsets and tightened back to the

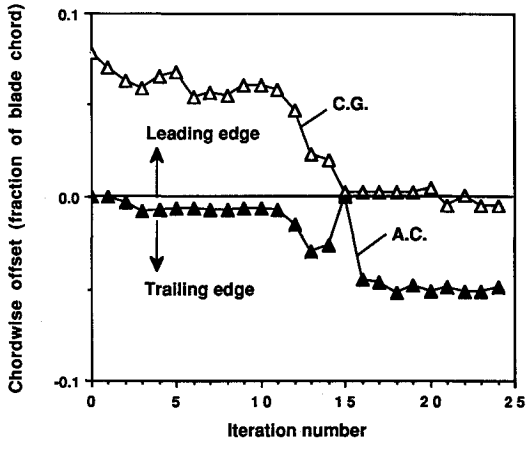

Fig. 10 Case 2—Iteration history of the blade chordwise offsets, stiff in-plane blade configuration.

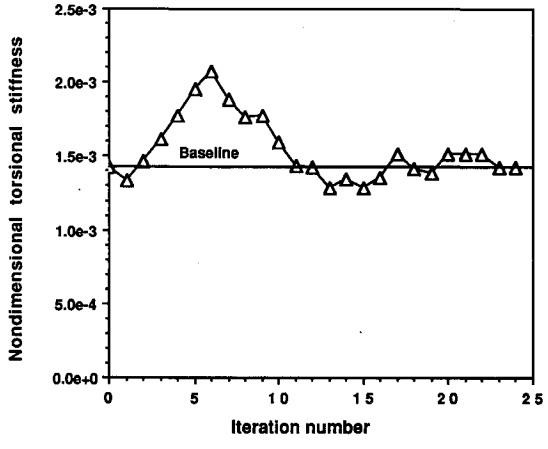

Fig. 11 Case 2—Iteration history of the blade torsional stiffness, stiff in-plane blade configuration.

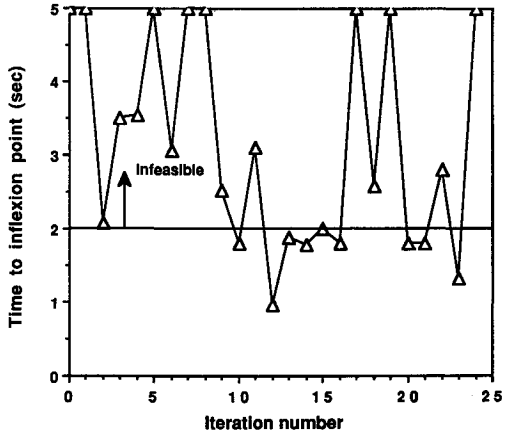

Fig. 12 Case 2—Iteration history of the time to inflexion point, stiff in-plane blade configuration.

original ±10% starting from design 17. The last two designs were not affected by the move limits.

Figure 9 underscores one of the weaknesses of the algorithm used in this study. Because the pseudo-Taylor expansions of the behavior constraints may not be very accurate locally and because the feasible directions-based optimizer[15,16] tends to follow closely the constraints while trying to minimize the objective function, not all the intermediate designs are feasible. It should be mentioned, however, that case 2 represents a rather difficult optimization problem because just three design variables with fairly limited ranges of variation are used to satisfy nine behavior constraints, some of which are quite severe. Methods that make the sequence of designs "funnel down the middle" of the feasible region have the potential for eliminating this problem and should be explored. These methods include the use of penalty functions[17] or the reformulation of the pseudo-Taylor series expansions using the hybrid approximations or Ref. 18.

Figure 10 shows that, for the initial iterations, the CG is placed in front of the elastic axis and the AC-EA offset x_A is very close to zero. As the optimization progresses, however, the EA is moved ahead of the AC and the CG becomes almost coincident with the EA. Overall, the chordwise distance between the CG and the AC tends to decrease. The

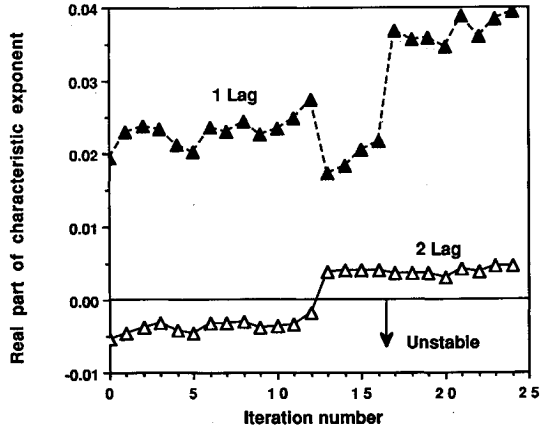

Fig. 13 Case 2—Iteration history of the damping of the first two lag modes, stiff in-plane blade configuration.

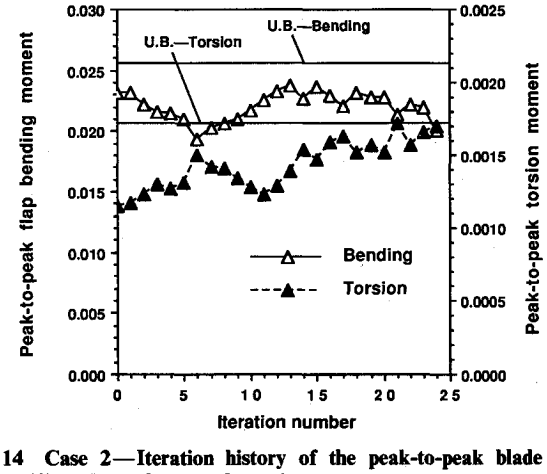

Fig. 14 Case 2—Iteration history of the peak-to-peak blade root loads, stiff in-plane blade configuration.

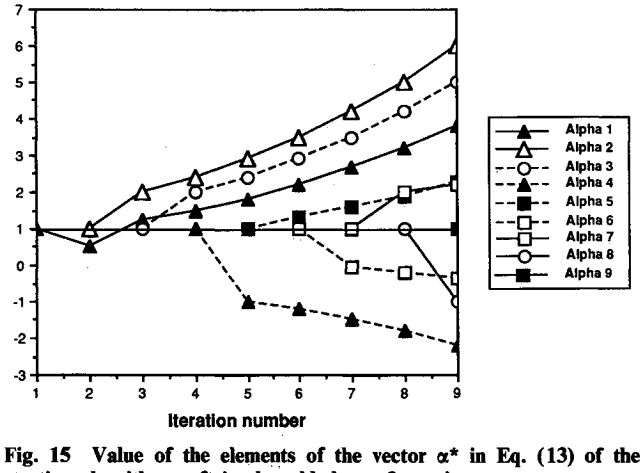

Fig. 15 Value of the elements of the vector α^* in Eq. (13) of the starting algorithm, soft in-plane blade configuration.

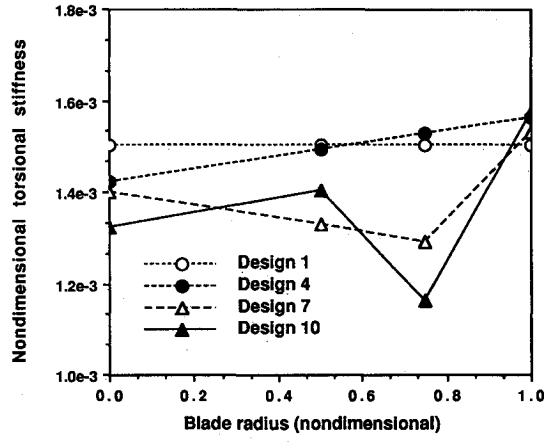

Fig. 16 Spanwise distribution of torsional stiffness GJ for four design vectors of the starting set, soft in-plane blade configuration.

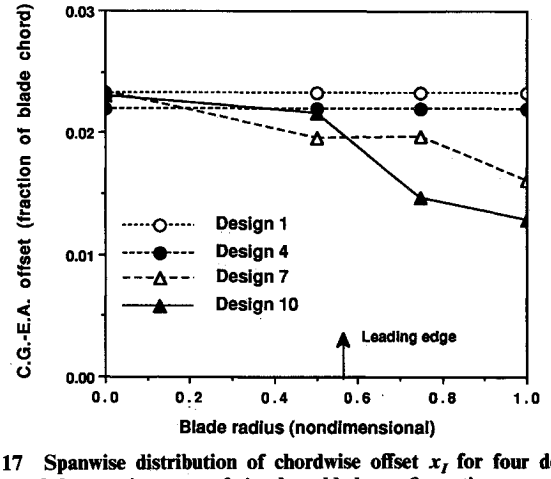

Fig. 17 Spanwise distribution of chordwise offset x_I for four design vectors of the starting set, soft in-plane blade configuration.

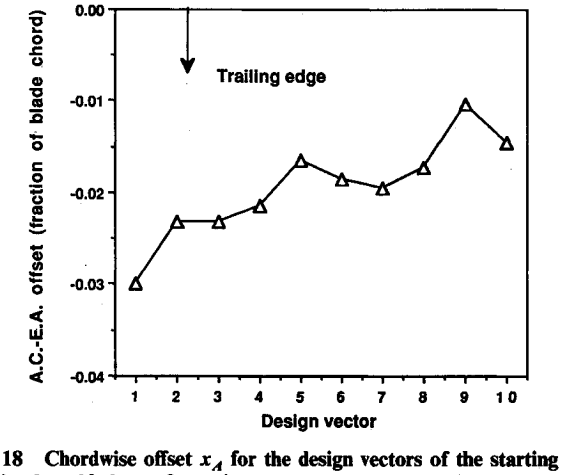

Fig. 18 Chordwise offset x_A for the design vectors of the starting set, soft in-plane blade configuration.

torsional stiffness GJ initially increases and subsequently tends to return to its baseline value, as shown in Fig. 11.

The iteration history of the time required to reach the inflexion point is shown in Fig. 12. One third of the designs do not exhibit an inflexion point at all: the arbitrary value of 5 s is assigned to these designs. The relatively large number of these designs complicates the task of generating high-quality approximations to the pitch response constraints and may be responsible for the poorer convergence properties of this example, compared with that of case 1. The first lag mode remains stable and its damping tends to increase during the optimization, as shown in Fig. 13. On the other hand, the second lag mode is slightly unstable throughout the first half of the optimization process. At design 13, the mode becomes stable and remains stable until the end of the optimization. As in case 1, the stability levels of the remaining four modes are much higher and remain high throughout the optimization. Therefore, no data for these modes are presented here. Finally, Fig. 14 presents the iteration histories of the root flap bending and torsion load constraints. The flap bending constraint is satisfied throughout the optimization, and the final design has peak-to-peak bending loads that are almost 20% lower than those of the initial design. On the other hand, the peak-to-peak torsion loads increase during the optimization. The final design has torsion loads that are about 50% higher than those of the initial design, and the corresponding behavior constraint is active or almost active for most of the last nine designs.

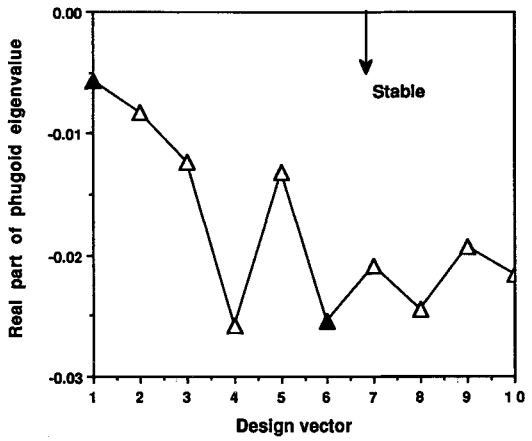

Fig. 19 Objective function for the design vectors of the starting set, soft in-plane blade configuration (solid symbols denote infeasible designs).

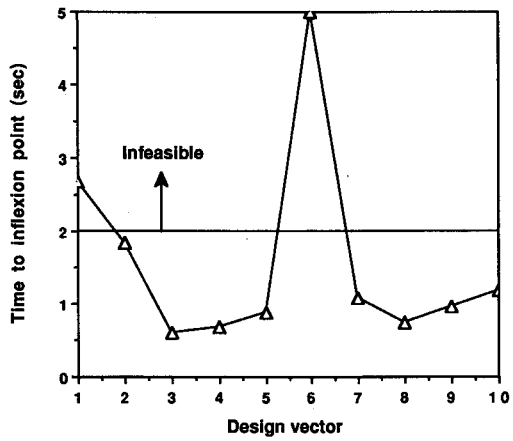

Fig. 20 Time-to-inflexion point for the design vectors of the starting set, soft in-plane blade configuration.

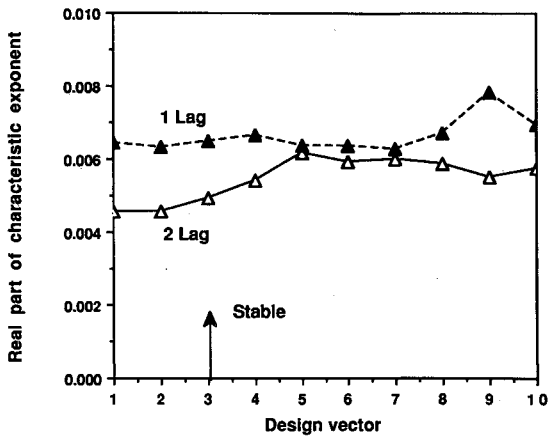

Fig. 21 Damping of the first two lag modes for the design vectors of the starting set, soft in-plane blade configuration.

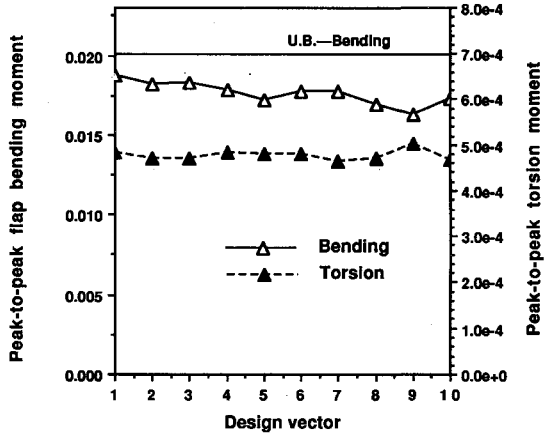

Fig. 22 Peak-to-peak blade root loads for the design vectors of the starting set, soft in-plane blade configuration.

Case 3: Determination of the Starting Set of Design Vectors

The third example focuses on the determination of the starting set of design vectors for a soft in-plane blade configuration similar to that of case 1. A total of nine design variables was used for this case, namely, the values of the torsional stiffness GJ at the root and the tip of the blade and at the 50% and 75% station, the values of the chordwise offset x_I at the same spanwise locations, and the value of the chordwise offset x_A, assumed to be constant along the blade. Thus, the starting set is composed of 10 design vectors.

The iteration history of the values of the elements of the vector α^* in Eq. (13) is shown in Fig. 15. The corresponding spanwise distributions of GJ and x_I are shown, respectively, in Figs. 16 and 17 for the four design vectors $\boldsymbol{D}_1$, $\boldsymbol{D}_4$, $\boldsymbol{D}_7$, and $\boldsymbol{D}_{10}$. The value of the chordwise offset x_A is shown in Fig. 18 for all of the design vectors.

Objective function and selected behavior constraints are shown in Figs. 19–22, respectively, for all the design vectors of the starting set. Figure 19 shows that, although the starting algorithm is not strictly an optimization algorithm, it is capable of generating high quality starting vectors. In fact, 8 of the 10 design vectors are feasible and all correspond to higher damping levels than the first vector $\boldsymbol{D}_1$. Six out of 10 generate at least four times as much damping than $\boldsymbol{D}_1$. The two infeasible designs violate the cyclic pitch response constraint, as shown in Fig. 20. The aeroelastic stability constraints are satisfied by all the designs. Figure 21 shows the real parts of the characteristic exponents of the two least damped modes, namely, the first two lag modes. The damping levels of the other four modes are much higher and are not

shown here. Finally, all designs satisfy the root load constraints; in Fig. 22 the upper bound on the torsion moments is outside the scale of the figure.

Conclusions

In evaluating and generalizing the conclusions that emerged from this numerical study, the underlying assumptions of the mathematical model and the parameters of the numerical study should be taken carefully into account. The results suggest the following:

1) The use of numerical optimization provides a powerful practical tool for an interdisciplinary dynamic design of the helicopter, which includes flight dynamics as well as rotor dynamics and aeroelasticity considerations.

2) It is possible to design both soft and stiff in-plane hingeless rotors that are aeroelastically stable, stabilize the longitudinal dynamics of the helicopter, and satisfy pitch response requirements. This is possible without additional stability and control augmentation systems and with a relatively small increase of blade root loads.

3) The final designs have the CG placed ahead of the EA and the AC behind it. The CG-EA chordwise offset x_I is close to zero for the stiff in-plane blade configuration.

4) The critical behavior constraint for both soft and stiff in-plane blade configurations is the cyclic pitch response requirement. The blade root load constraints may become critical for both configurations if too small an increase is allowed during the optimization process. The aeroelastic stability of the second lag mode is critical only for the stiff in-plane blade configuration.

5) The optimization procedure described in this study is efficient and requires a relatively small number of analyses to generate acceptable designs. If a starting set of design vectors is not already available, the algorithm presented in the paper can generate high quality initial designs.

4) A drawback of the optimization procedure is that not all the intermediate designs are feasible. This is because the feasible directions-based optimizer tries to follow closely behavior constraints that may not always be approximated accurately. The use of formulations and optimizers that tend to funnel down the middle of the feasible region should remove this problem and will be explored in the future.

Acknowledgments

This work was supported by NASA Langley Research Center under Grant NAG-1-739, technical monitor Joanne Walsh. This work was initiated with the support of the Army Research Office, Contract DAAL-03-88-C-002, technical monitor Robert Singleton. The starting algorithm is based on ideas suggested to the author by Lucien A. Schmit, Jr. The support of the Computer Science Center of the University of Maryland, where all of the calculations were performed, is also acknowledged.

References

[1]Davis, M. W., and Weller, W. H., "Application of Design Optimization Techniques to Rotor Dynamics Problems," *Journal of the American Helicopter Society*, Vol. 33, No. 3, 1988, pp. 42–50.

[2]Celi, R., and Friedmann, P. P., "Structural Optimization with Aeroelastic Constraints of Rotor Blades with Straight and Swept Tips," *AIAA Journal*, Vol. 28, No. 5, 1990, pp. 928–936.

[3]Lim, J. W., and Chopra, I., "Aeroelastic Optimization of a Helicopter Rotor," *Journal of the American Helicopter Society*, Vol. 34, No. 1, 1989, pp. 52–62.

[4]Walsh, J. L., Bingham, G. J., and Riley, M. F., "Optimization Methods Applied to the Aerodynamic Design of Helicopter Rotor Blades," AIAA Paper 85-0644, April 1985.

[5]Kumar, S., and Bassett, D., "Rotor Performance Optimization for Future Light Helicopter," 43rd Annual Forum of the American Helicopter Society, St. Louis, MI, May 1987, pp. 345–355.

[6]Schmit, L. A., Jr., and Miura, H., "Approximation Concepts for Efficient Structural Synthesis," NASA CR-2552, 1976.

[7]Vanderplaats, G. N., "Approximation Concepts for Numerical Airfoil Optimization," NASA TP-1370, March 1979.

[8]Chattopadhyay, A., and Walsh, J. L., "Minimum Weight Design of Helicopter Rotor Blades with Frequency Constraints," *Journal of the American Helicopter Society*, Vol. 34, No. 2, 1989, pp. 77–82.

[9]Celi, R., and Friedmann, P. P., "Rotor Blade Aeroelasticity in Forward Flight with an Implicit Aerodynamic Formulation," *AIAA Journal*, Vol. 26, No. 12, 1988, pp. 1425–1433.

[10]Celi, R., "Effect of Hingeless Rotor Aeroelasticity on Helicopter Trim and Longitudinal Stability Using Quasilinearization," AIAA Paper 88-4366, Aug. 1988.

[11]Celi, R., "Aeroelastic Effects on Stability and Control of Hingeless Rotor Helicopters," Paper No. 76, Fourteenth European Rotorcraft Forum, Milano, Italy, Sept. 1988.

[12]Bramwell, A. R. S., *Helicopter Dynamics*, Edward Arnold, London, 1976.

[13]Johnson, W., *Helicopter Theory*, Princeton Univ., Princeton, NJ, 1980, pp. 861–862.

[14]"MIL-H-8501A—Military Specification—Helicopter Flying and Ground Handling Qualities; General Requirements for," Sept. 1961, pp. 3–4.

[15]Vanderplaats, G. N., and Moses, F., "Structural Optimization by Methods of Feasible Directions," *Journal of Computers and Structures*, Vol. 3, July 1973, pp. 739–755.

[16]Vanderplaats, G. N., "CONMIN—A FORTRAN Program for Constrained Function Minimization; User's Manual," NASA TM-X-62,282, Aug. 1973.

[17]Fox, R. L., *Optimization Methods for Engineering Design*, Addison-Wesley, Reading, MA, 1971.

[18]Fleury, C., and Braibant, V., "Structural Optimization: A New Dual Method Using Dual Variables," *International Journal for Numerical Methods in Engineering*, Vol. 24, 1987, pp. 409–428.